Article

Detailed Investigation of the Eddy Current and Core Losses in Coaxial Magnetic Gears through a Two-Dimensional Analytical Model

Nikolina Nikolarea [1], Panteleimon Tzouganakis [2,*], Vasilios Gakos [1], Christos Papalexis [2], Antonios Tsolakis [2] and Vasilios Spitas [1]

1   Laboratory of Machine Design, National Technical University of Athens, 9 Iroon Polytechniou, 15780 Zografou, Greece; nikolareanikol@gmail.com (N.N.); vgakos@mail.ntua.gr (V.G.); vspitas@mail.ntua.gr (V.S.)
2   Laboratory of Machine Elements and Vehicles, University of West Attica, 250 Thivon & P. Ralli, 12244 Egaleo, Greece; chpapalexis@uniwa.gr (C.P.); adtsolakis@uniwa.gr (A.T.)
*   Correspondence: ptzouganakis@uniwa.gr

Abstract: This work introduces a 2D model that calculates power losses in coaxial magnetic gears (CMGs). The eddy current losses of the magnets are computed analytically, whereas the core losses of the ferromagnetic segments are computed using an analytical–finite element hybrid model. The results were within 1.51% and 3.18% of those obtained from an FEA for the eddy current and core losses in the CMG for an indicative inner rotor speed of 2500 rpm. In addition, the significance of the circumferential magnet segmentation is demonstrated in the CMGs. Furthermore, a parametric investigation of the efficiency of the system for different applied external loads is carried out. Finally, a mesh sensitivity analysis is performed, along with the computation of the average power losses throughout one full period, resulting in an at least 80% reduction in computational costs with a negligible effect on accuracy. The developed model could be a valuable tool for the minimization of power losses in CMGs since it combines high accuracy with a low computational cost.

1. Introduction

Mechanical gears have been one of the main machine elements used for power transmission and speed and torque conversion since the Industrial Revolution. Teeth geometry and the materials used have been researched extensively in order to achieve both a high torque density and high efficiency. However, they are still prone to problems, such as surface and bending fatigue, wear, noise, and the need for lubrication and maintenance [1]. However, magnetic gears that utilize permanent magnets (PMs) are characterized by a high reliability due to the lack of contact and friction between their rotating parts. It has also been shown that they can achieve high efficiency and a high torque density, while being compact and producing essentially zero torque ripple [2]. However, their efficiency diminishes at high rotational speeds.

Coaxial magnetic gears (CMGs) were first introduced two decades ago by Atallah et al. [3], and since then there has been a growing interest in their use in different applications, including power generation [4,5] and aerospace [6]. The analytical solutions of the scalar magnetic potential of CMGs and the subsequent magnetic flux densities and induced torques in the two rotors were computed analytically by Tzouganakis et al. [7]. However, significant issues regarding the torque density, the slippage, and power losses due to eddy currents are present in CMGs, which limit their wider application in the industry [7]. In particular, eddy current losses have been a significant issue in CMGs, especially at higher rotational speeds [1]. Therefore, it is essential to investigate this phenomenon during the

design of CMG drives, since excess eddy current losses could lead to increases in the temperature and deterioration of the PMs in the rotors, which could gradually lead to degradation of the system as a whole.

In general, the calculation of the eddy current and core losses is a strenuous process that requires complex transient electromagnetic phenomena. Desvaux et al. [8] and Wang et al. [9] computed the eddy current losses of PMs by first calculating the square of the current density throughout the PMs, multiplying this by the resistivity, performing a volume integration, and finally integrating this with respect to time and dividing it by the period of the system to obtain the average value of the eddy current losses. They also performed circumferential magnet segmentation to decrease the eddy current losses by performing a volume integration on each segment separately. Filippini [10] performed both circumferential and axial magnet segmentation and correlated the eddy current losses and the number of segments to a rational function. Regarding core losses, Filippini [10] starts with the computation of the flux density throughout the ferromagnetic segments, with a simple finite-difference model that utilizes the boundary scalar magnetic potential conditions and the Laplace equation using cylindrical coordinates. Core losses, according to Deng [11], require using the rate of change in the flux density to calculate hysteresis, the eddy current, and excess losses. Deng introduced a formula to calculate these losses while including the harmonic effect. Desvaux et al. [8] used this formula to perform core loss calculations. Hein et al. [12] reviewed different approaches to the Steinmetz equation, which calculates hysteresis losses. Lee et al. [13] and Li et al. [14] proposed that, for the same magnitude of flux density, the rotational core losses are almost double the alternating core losses. Mateev and Marinova [15] calculated the eddy current losses of a CMG at different rotational speeds and showed that high rotational speeds result in non-negligible losses as a percentage of the total transmitted power.

The calculation of the power losses is a computationally high process, as it requires the calculation of the magnetic flux density at different angles of rotation of the rotors of the CMG. FE models, despite having high accuracy, require significant computational time. As a consequence, an optimization process in order to minimize the power losses could potentially be a time-consuming procedure. Therefore, a model which utilizes analytical solutions of the magnetic flux density in the CMG could significantly reduce the computational cost and facilitate optimization processes and could become a valuable design tool.

This work focuses on the computation of PM and ferromagnetic segment losses. The analytical solutions of the scalar magnetic potential, which are derived from Maxwell's equations, are used to calculate the current density and thus the eddy current losses of the PMs. Circumferential segmentation is also performed to investigate its impact regarding loss reduction. Core losses are determined using a hybrid analytical–finite element model that utilizes the boundary scalar magnetic potential conditions. The resulting PMs and core losses were in excellent coherence with the FEA results, while circumferential segmentation greatly improved the PMs' efficiency. In addition, an investigation on the effect of different applied external loads on the PMs' efficiency is conducted. Finally, a study on the average power losses throughout one full period is conducted, along with a mesh sensitivity analysis in order to reduce the computational time without losing accuracy in the obtained results. From the conducted analysis, it was demonstrated that the computational time can be reduced up to 80%. The mesh sensitivity analysis showed that mesh resolution is crucial for accurate core loss calculation, as meshes that are too coarse result in inaccurately high core losses while meshes that are too fine result in high computational costs. These two analyses are of great importance, as they ensure high accuracy and relatively low computational costs simultaneously, facilitating optimization efforts.

2. Mathematical Modeling

2.1. Principles of CMGs

To couple the rotors, it is necessary for the number of ferromagnetic segments, Q, in the flux-modulator ring to be equal to the sum of pole pairs of PMs, as shown in Equation (1).

$$p_{in} + p_{out} = Q \tag{1}$$

In the case discussed in the paper, where the flux-modulator ring is fixed, the gear ratio G_M is calculated as in Equation (2) [2,8].

$$G_M = -\frac{p_{out}}{p_{in}} \tag{2}$$

A typical CMG is presented in Figure 1. The CMG consists of two concentric iron yokes (rotors) with PMs (permanent magnets) mounted on them, as well as a fixed flux-modulator ring between the yokes. The north and south poles of the PMs are colored in red and blue, respectively.
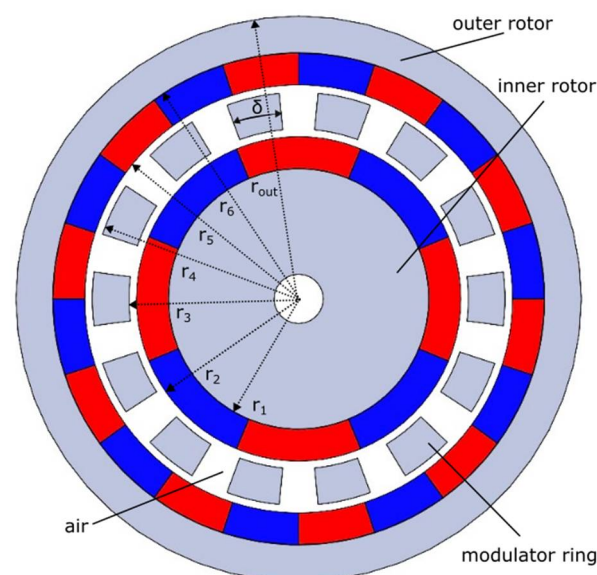
Figure 1. Coaxial magnetic gear (CMG).

The main parts are the inner and outer rotor and the modulator ring. As shown in Figure 1, $r_1, r_2, r_3, r_4, r_5, r_6$, and r_{out} are the radii of the inner iron yoke, the inner permanent magnets, the inner modulator ring's side, the outer modulator ring's side, the outer permanent magnets, the outer iron yoke and the outer side of the coaxial magnetic gear, respectively. In addition, δ is the angle of each ferromagnetic segment.

2.2. Computation of Eddy Current Losses of PMs Using a 2D Analytical Model

For the calculation of the PM losses, the vector magnetic potential A throughout the PMs is required. The vector magnetic potential can be easily determined after the scalar magnetic potential φ calculation. The scalar magnetic potential is computed by dividing the CMG into regions, calculating the φ produced by each rotor PM to all regions, and superimposing them [7]. In Figure 2, the model that refers to the effect of the inner PMs is illustrated. Region I represents the inner rotor PMs, Region II represents the airgap between the inner rotor and the modulator ring, and Region III represents the space between the modulator ring and the outer diameter of the outer PMs. The same approach is used for the model that refers to the effects of the outer rotor [7].
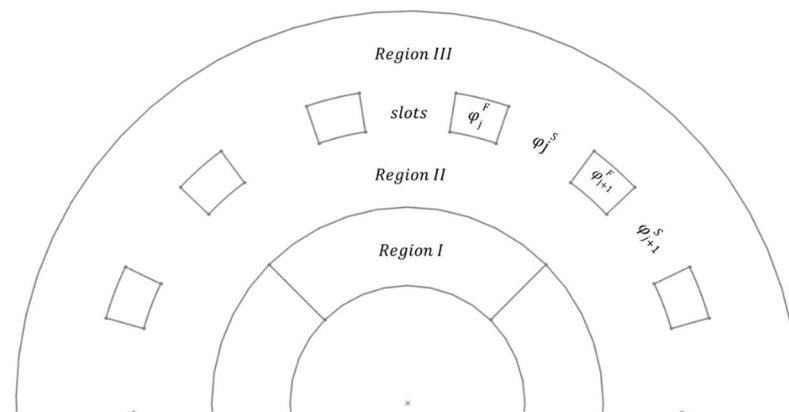
Figure 2. Regions of the analytical model used for calculating inner PM effects [7].

The scalar magnetic potential in each region is calculated using partial differential Equations (3) and (5) derived from Maxwell's equations (Gauss and Ampere Law). It is noted that the assumption of infinite permeability of the iron yokes and the ferromagnetic segments $\left(\varphi_j^F \right)$ is considered [7].

$$\nabla^2 \varphi^I(r,\theta) = \frac{div\boldsymbol{M}}{\mu_r} \ in \ Region \ I \tag{3}$$

$$\nabla^2 \varphi^{II,III}(r,\theta) = 0 \ in \ Regions \ II, \ III \tag{4}$$

$$\nabla^2 \varphi^S(r,\theta) = 0 \ in \ the \ slots \tag{5}$$

where $\boldsymbol{M}$ is the magnetization vector of the PMs. The vector magnetic potential $\boldsymbol{A}$ can be determined, using Equations (6) and (7).

$$B_r^k(r,\theta) = -\mu_0 \frac{\partial \varphi^k}{\partial r} = \frac{1}{r} \frac{\partial \boldsymbol{A}^k}{\partial \theta} \tag{6}$$

$$B_\theta^k(r,\theta) = -\mu_0 \frac{\partial \varphi^k}{\partial \theta} = -\frac{\partial \boldsymbol{A}^k}{\partial r} \tag{7}$$

where B_r^k and B_θ^k are the radial and tangential flux density of a point of the inner and outer rotor (*k:in* or *out*), r and θ refer to the polar coordinates, and μ_0 is the vacuum permeability.

The eddy current losses for each PM are computed using Equations (8)–(10) [8,9].

$$P_{eddy}^k = \frac{L}{\Theta_p^k} \int_0^{\Theta_p^k} \frac{1}{\sigma} \int_{S_{PM}^k} \left(\left(J^k \right)^2 r dr d\theta \right) d\theta_0^k \tag{8}$$

$$J^k \left(r, \theta, \theta_0^k \right) = \sigma \omega^k \frac{\partial \boldsymbol{A}^k}{\partial \theta_0^k} + C^k(\theta_0^k) \tag{9}$$

$$C^k \left(\theta_0^k \right) = -\frac{1}{S_{PM}^k} \int_{S_{PM}^k} \sigma \omega^k \frac{\partial \boldsymbol{A}^k}{\partial \theta_0^k} r dr d\theta \tag{10}$$

where J^k is the eddy current density, C^k is a term used to guarantee that the net current flowing in each PM arc segment is zero at any moment, S_{PM}^k is the area of a PM, and σ is the conductivity of the PMs. In addition, θ_0^k and ω^k refer to the angle of rotation and the rotational speed of each rotor, while Θ_p^k is the angle that each rotor rotates in a complete period of the system.

For the calculation of Θ_p^k, the greatest common divisor of the pole pairs p_{in} and p_{out} is found, and then the pole pairs are divided by it. The result of this simple operation is the number of revolutions the outer and inner rotor complete in a period, respectively. For

example, if $p_{in} = 4$ and $p_{out} = 10$, this means that the inner rotor completes 5 revolutions and the outer rotor completes 2 revolutions in a period, resulting in $\Theta_p^{in} = 10\pi \ rad$ and $\Theta_p^{out} = 4\pi \ rad$.

The computations are performed for the case of a full load, which refers to the case of the torque transmitted being equal to the stall torque. This is ensured by choosing the appropriate initial position of the two rotors, according to Equations (11) and (12) [7].

$$M_{in} = M_{stall,in}\sin\left(p_{in}\theta_{in} + p_{out}\theta_{out}\right) \tag{11}$$

$$M_{out} = -M_{stall,out}\sin\left(p_{in}\theta_{in} + p_{out}\theta_{out}\right) \tag{12}$$

where θ_{in} and θ_{out} are the positions of the two rotors and $M_{stall,in}$ and $M_{stall,out}$ are their stall torque, which are calculated analytically in [7]. In this study, in order to achieve stall torque, θ_{out} is initialized as zero, and θ_{in} is calculated to be equal to 22.5°.

2.3. Circumferential Segmentation of PMs

Eddy currents losses in PMs can be reduced with axial or circumferential segmentation. The present work focuses on circumferential segmentation. Incorporating circumferential segmentation into the analytical model requires dividing the angle by the number of total segments (K_{in}, K_{out}), as shown in Equation (13) [9] for each rotor.

$$\theta \in \left[\theta_0, \theta_0 + \frac{\pi}{p_{in}}\frac{1}{K_{in}}\right], \ \theta \in \left[\theta_0, \theta_0 + \frac{\pi}{p_{out}}\frac{1}{K_{out}}\right] \tag{13}$$

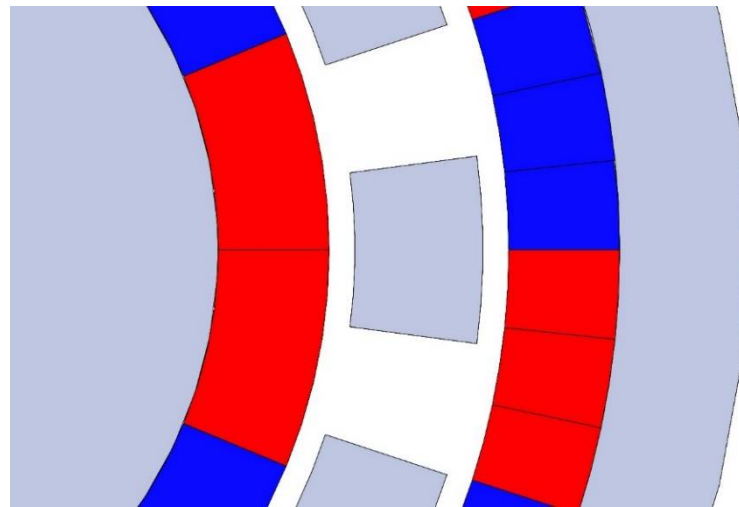An example of circumferential segmentation is presented in Figure 3.

Figure 3. Illustration of magnet segmentation ($K_{int} = 2$ and $K_{out} = 3$).

2.4. Computation of Core Losses of the Ferromagnetic Segments Using a Hybrid Model

In a special case of sinusoidal variation in the magnetic fields, core losses are calculated using Equation (14) [8].

$$P_{core,sinusoidal} = n\left(k_{hyst}f^{\alpha}B_m^{\beta} + k_{eddy}f^2 B_m^2 + k_{exc}f^{1.5}B_m^{1.5}\right) \tag{14}$$

where f and B_m are the frequency and peak value of the flux density, respectively, and α, β, k_{hys}, k_{eddy}, and k_{exc} are constants that depend on the material and are provided by the manufacturer. Rotational fields result in core losses that are double those produced from alternating fields [13,14]. This is denoted in Equation (14) with the variable n, which has a value of 1 when referring to alternating fields and 2 when referring to rotating fields, as in this case.

In general, fields in CMGs do not appear with a strict sinusoidal variation, so a generalized equation is used to calculate the core losses, as shown in Equations (15) and (16) [8,11,12].

$$
\begin{aligned}
P^F_{eddy} &= P_{core,generalised} \\
&= L \int_{S_{fer}} n\left(\frac{k'_{hyst}}{T} \int_O^T \left| \sqrt{\left(\frac{dB_{maj}}{dt}\right)^2 + \left(\frac{dB_{min}}{dt}\right)^2} \right|^\alpha \left| \sqrt{B_{maj}^2 + B_{min}^2} \right|^{\beta-\alpha} dt + \frac{k'_{eddy}}{T}\int_0^T \left(\left(\frac{dB_{maj}}{dt}\right)^2 + \left(\frac{dB_{min}}{dt}\right)^2 \right) dt \right. \\
&\left. + \frac{k'_{exc}}{T}\int_0^T \left(\left(\frac{dB_{maj}}{dt}\right)^2 + \left(\frac{dB_{min}}{dt}\right)^2 \right)^{0.75} dt \right) r\,dr\,d\theta
\end{aligned}
\tag{15}
$$

$$
\begin{cases}
k'_{hyst} = \dfrac{k_{hyst}}{2^{\beta-\alpha}(2\pi)^{\alpha-1}\int_0^{2\pi}|cos\theta|^\alpha dt} \\[2mm]
k'_{eddy} = \dfrac{k_{eddy}}{2\pi^2} \\[2mm]
k'_{exc} = \dfrac{k_{exc}}{(2\pi^2)^{0.75}}
\end{cases}
\tag{16}
$$

where B_{maj} and B_{min} represent the major and minor axes of the ellipse fitted to the flux density locus, S_{fer} refers to the area of a segment, and T is a complete period of the system.

$B_{maj}(t)$ and $B_{min}(t)$ are the components of $B(t)$ along the axes of the ellipse, and they are calculated using Equations (17)–(20).
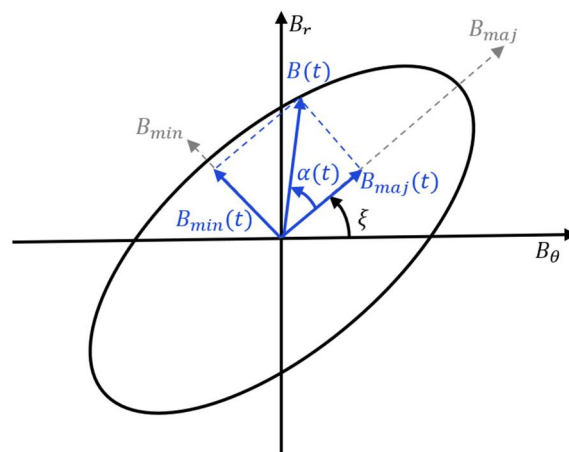
$$
B_{maj}(r,\theta,t) = \|B(r,\theta,t)\|\cos(a(t))
\tag{17}
$$

$$
B_{min}(r,\theta,t) = \|B(r,\theta,t)\|\sin(a(t))
\tag{18}
$$

$$
\xi(r,\theta) = \arctan\left(\frac{B_r\left(r,\theta,t_{max\|B(r,\theta,t)\|}\right)}{B_\theta\left(r,\theta,t_{max\|B(r,\theta,t)\|}\right)} \right)
\tag{19}
$$

$$
a(r,\theta,t) = \arctan\left(\frac{B_r(r,\theta,t)}{B_\theta(r,\theta,t)} \right) - \xi(r,\theta)
\tag{20}
$$

where ξ and $a(t)$ are defined in Figure 4.

Figure 4. A sketch of the fitted ellipse, along with the parameters required for core loss calculations.

In order to calculate the core losses, the values of B_r and B_θ on the ferromagnetic segment's surface should be calculated. However, the analytical model developed in [7] does not calculate the scalar magnetic potential of the segments, but it does calculate the magnetic potential on their boundaries. Those analytically calculated values can be used

as boundary conditions for a finite element model. This model makes use of Laplace's equation of the scalar magnetic potential φ using a cylindrical coordinate system [10].

$$\frac{\partial^2 \varphi}{\partial r^2} + \frac{1}{r}\frac{\partial \varphi}{\partial r} + \frac{1}{r^2}\frac{\partial^2 \varphi}{\partial \theta^2} = 0 \tag{21}$$

A grid is created using the reference system shown in Figure 5. The average radius r_i and angle θ_j of each module are calculated as in Equations (22) and (23), where $\Delta r = (r_4 - r_3)/N$ and $\Delta \theta = \delta/N$, where N is the number of rows and columns of the finite element grid.

$$r_i = r_4 - \left(i - \frac{1}{2}\right)\Delta r \tag{22}$$

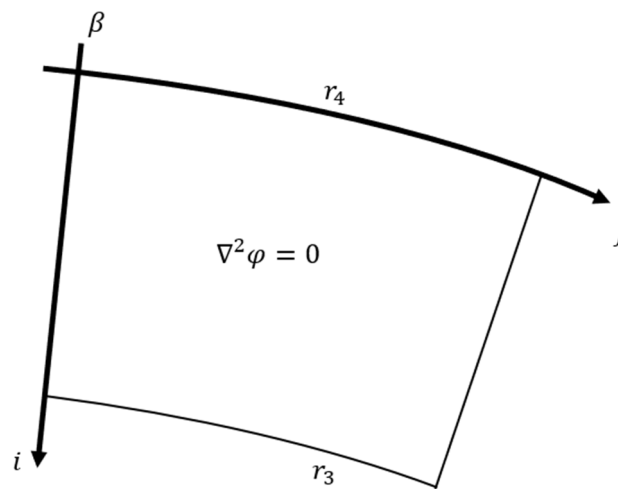$$\theta_j = \beta - \left(j - \frac{1}{2}\right)\Delta \theta \tag{23}$$

Figure 5. The reference system of the finite element grid.

Using central finite differences, Laplace's equation leads to a system of N^2 equations, presented in Equations (24) and (26).

$$D_{N^2 x N^2}\, \Phi_{N^2 x 1} = R_{N^2 x 1} \tag{24}$$

For all (i, j) pairs where $i = 1$ or $i = N$ or $j = 1$ or $j = N$, the corresponding modules of D, Φ, and R are assigned values according to Equation (25), where $\varphi(r_i, \theta_j)$ is the boundary condition. For the rest of the (i, j) pairs, Equation (26) is followed.

$$\begin{cases} D_{(i-1)N+j,(i-1)N+j} = 1 \\ R_{(i-1)N+j,1} = \varphi(r_i, \theta_j) \end{cases} \tag{25}$$

$$\begin{cases} D_{(i-1)N+j,(i-1)N+j} = -\frac{2}{\Delta r^2} - \frac{2}{r^2 \Delta \theta^2} \\ D_{(i-1)N+j,(i-1)N+j+1} = \frac{1}{r^2 \Delta \theta^2} \\ D_{(i-1)N+j,(i-1)N+j-1} = \frac{1}{r^2 \Delta \theta^2} \\ D_{(i-1)N+j,(i-1)N+j+N} = \frac{1}{\Delta r^2} + \frac{1}{2r\Delta r} \\ D_{(i-1)N+j,(i-1)N+j-N} = \frac{1}{\Delta r^2} - \frac{1}{2r\Delta r} \\ R_{(i-1)N+j,1} = 0 \end{cases} \tag{26}$$

Solving for $\Phi_{N^2 x 1}$ returns the scalar magnetic potential $\varphi(r_i, \theta_j)$ on every module of the grid. B_r and B_θ on the ferromagnetic segment can now be calculated using Equations (6) and (7), and the core losses can be calculated using Equations (15)–(20).

3. Results and Discussion

3.1. Eddy Current and Core Loss Calculation and Comparison with FEA

A case study is performed with the parameters described in Table 1. The rotational speed of the inner rotor is assumed to be 2500 rpm. The time step used is equal to the time it takes for the inner rotor to rotate by 2° or, equivalently, for the outer rotor to rotate by 0.8°. This time step allows for high-accuracy computations and simultaneously limits the amount of time steps in one period. The computations are performed for the case of a full load. An algorithm based on the developed model is constructed in MATLAB. The results were compared to those obtained from the FE transient analysis performed in the Ansys Maxwell 2023 R1 software.

Table 1. Parameters of the CMG example used for the calculations.

p_{in}	Number of inner ring pole pairs	4
p_{out}	Number of outer ring pole pairs	10
Q	Number of ferromagnetic segments	14
r_1	Inner radius of inner ring	53 mm
r_2	Outer radius of inner ring	66 mm
r_3	Inner radius of flux-modulator ring	69 mm
r_4	Outer radius of flux-modulator ring	84 mm
r_5	Inner radius of outer ring	87 mm
r_6	Outer radius of outer ring	87 mm
L	Length	100 mm
δ	Ferromagnetic segment angle	15°
B_r	Residual flux density of magnets	1.47 T
μ_0	Vacuum magnetic permeability	$4\pi \cdot 10^{-7}$ Hm^{-1}
$\mu_r^I = \mu_r^{III}$	Relative permeability of the magnets	1.05
σ	Conductivity of the magnets	0.9 MS/m

Figure 6a shows that the eddy current losses of the PMs are proportional to the square of the rotational speed of the rotors, while Figure 6b shows that the percentage of eddy current losses to total transmitted power is proportional to the rotational speed of the rotors, as expected from Equations (8)–(10).
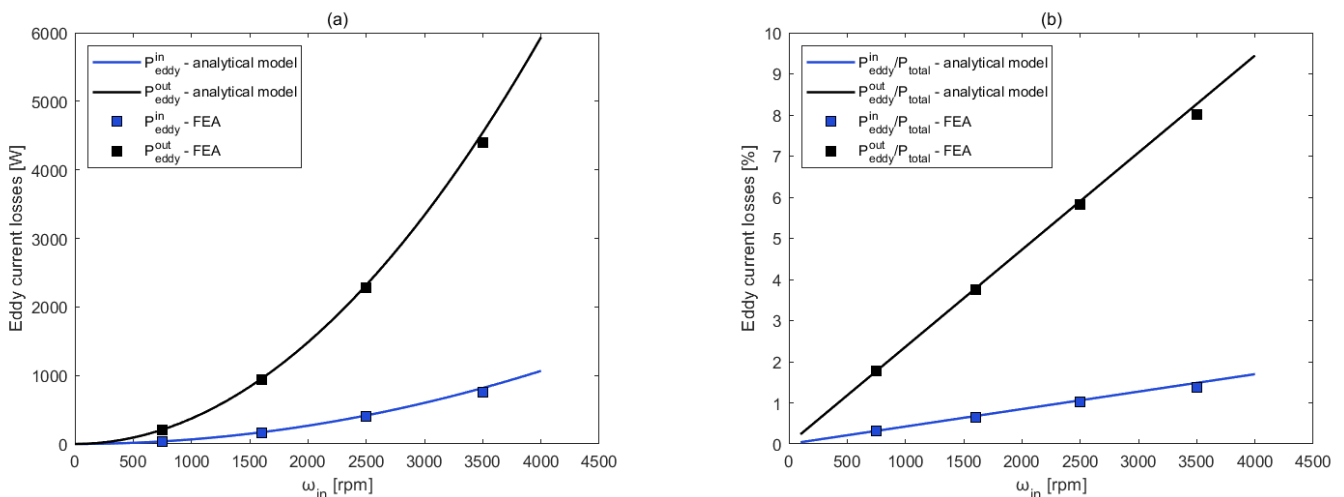
Figure 6. Comparison of results obtained from the analytical model and the 2D finite element analysis model regarding the (**a**) eddy current losses and (**b**) percentage of eddy current losses to total transmitted power.

It is observed that the eddy current losses on the outer rotor are higher compared to the inner rotor, a result that is in coherence with similar studies in the literature [8,10].

In addition, for an inner rotational speed greater than 2000 rpm, the total eddy current losses in the PMs exceed 5% of the total transmitted power, illustrating the drawback of CMGs at high rotational speeds, which has also been reported in the literature [1]. The analytical results of the developed model were verified with an FEA. The discrepancies between the analytical model and the FEA simulations are small and of the same nature for both rotors. For slower rotational speeds, the analytical model results in slightly less eddy current losses, 0.01% for the inner rotor and 0.9% for the outer rotor PMs, which are less than the FEA simulations for an inner rotational speed of 750 rpm. As rotational speeds increase, the analytical model results in larger eddy current losses, reaching deviances of 7.8% and 3.1% for the inner and outer rotor PMs, respectively, for an inner rotational speed of 3500 rpm. In Figure 7, the distribution of the eddy current density throughout a PM at a random time of operation, as calculated from the FEA simulation, is presented.
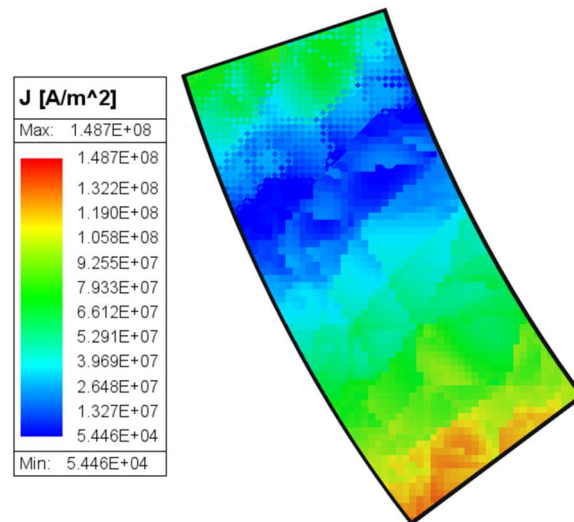

Figure 7. Eddy current density distribution on a PM.

Figure 8 shows the effect of magnet segmentation on the eddy current losses. The losses decrease rapidly in the outer rotor and more slowly in the inner rotor, as circumferential segments increase. According to Filippini [10], the eddy current losses should follow the function $P_{eddy}(K_k) = \frac{c}{a^2 + b^2 K_k^2}$, where K_k is the number of circumferential segments of every PM of a rotor and a, b, c are constants.
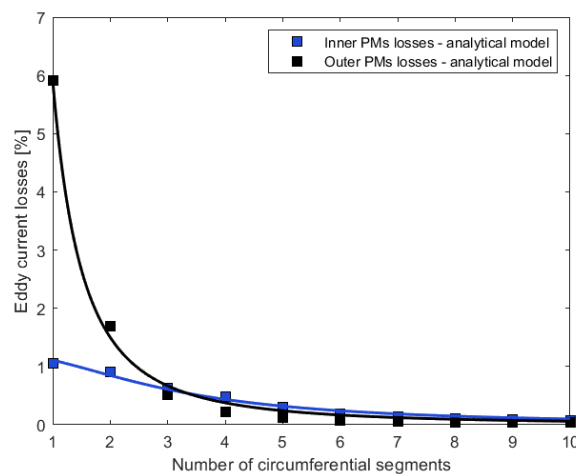

**Figure 8.** Circumferential segmentation effects on the eddy currents losses of the PMs.

Fitting this function results in a coefficient of determination of $R^2 = 0.9842$ and $R^2 = 0.9963$ for the inner and outer PM losses, while the values of a, b, and c are equal to 0.115, 0.039, and 0.016 for the inner PMs and 0.031, 0.215, and 0.280 for the outer PMs, respectively.

For the calculation of the core losses, some additional parameters are required and are presented in Table 2.

Table 2. Parameters used in this case study for the calculation of core losses.

k_h	Hysteresis loss coefficient	152.2 $WsT^{-\beta}$ m^{-3}
k_{ed}	Eddy current loss coefficient	0.403 Ws^2T^{-2} m^{-3}
k_{ex}	Excess loss coefficient	0.1 $Ws^{1.5}T^{-1.5}$ m^{-3}
α	Steinmetz coefficient	1
β	Steinmetz coefficient	2

The flux density locus of a single finite element of a ferromagnetic segment and its fitted ellipse is presented in Figure 9. The major and minor axes are calculated using Equations (17)–(20).
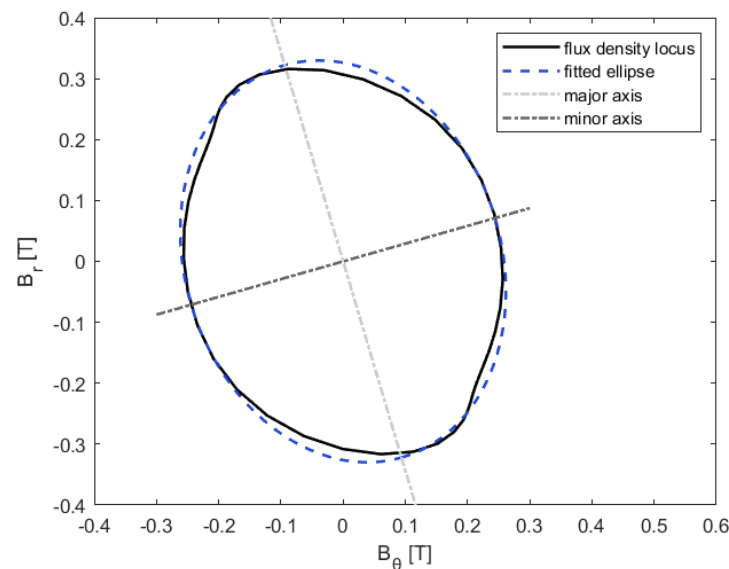
Figure 9. The flux density locus of a finite element of a ferromagnetic segment, the fitted ellipse, and its axes.

The resulting flux density of the proposed hybrid model on a ferromagnetic segment at a random point in time is shown in Figure 10. For the calculation of the core losses, a 60×60 mesh grid is used.

Flux density is generally close to zero and smooth, except for some small areas around the edges, and especially the corners, where it can reach values as high as 2.5T.

Figure 11a,b compare the computed results to those obtained using the FEA for various rotational speeds.

Core losses were found to be one order of magnitude less than the inner PM losses and two orders of magnitude less than the outer PM losses. Specifically, the core losses do not exceed 0.2% of the total transmitted power, even at high rotational speeds. The results of the analytical model were compared to those obtained from the FEA. Higher discrepancies in core losses between the results from the hybrid model and the FEA software for lower rotational speeds, that are further highlighted in Figure 11b, can be attributed to the overall lower losses, which make slight deviations stand out. However, the discrepancies do not surpass 10% for an inner rotational speed greater than 500 rpm, and they decrease, percentage-wise, as the rotational speeds increase.
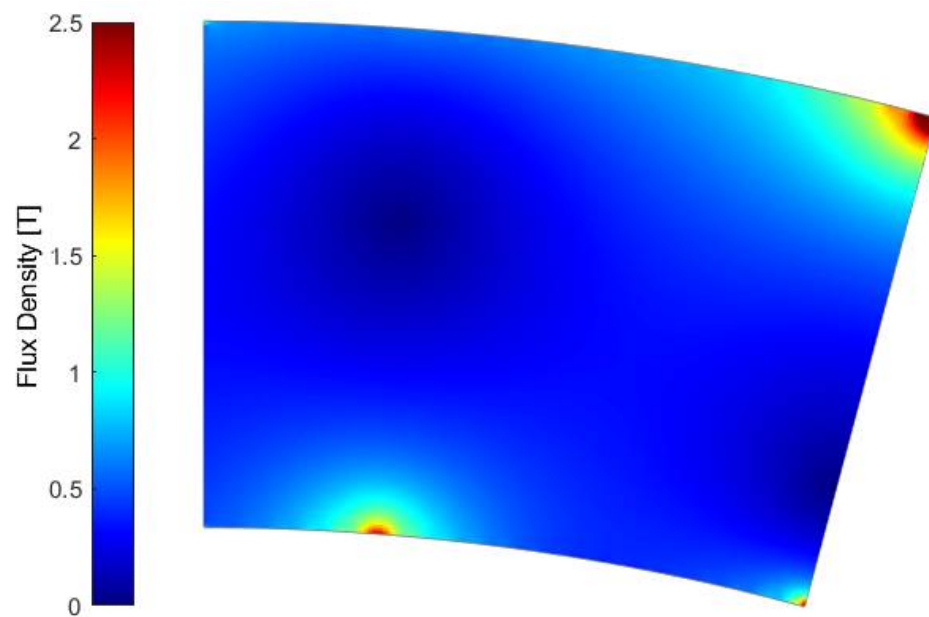
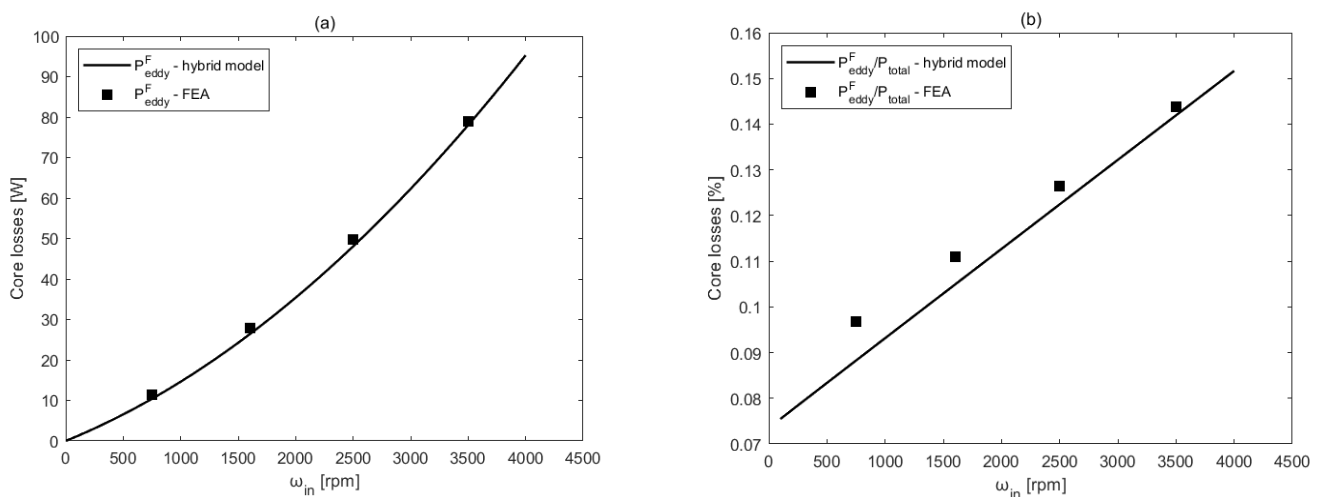**Figure 10.** Flux density distribution on a ferromagnetic segment.

Figure 11. Comparison of results obtained from the hybrid model and the 2D finite element analysis model regarding (**a**) core losses and (**b**) the percentage of core to total transmitted power.

3.2. Power Losses for Different External Loads

Different external loads result in different relative positions of the two rotors. It would be interesting to investigate how and if the transmitted load has any effect on the power losses of the CMG. To simplify the calculations, θ_{out} is initialized as zero and θ_{in} is assigned different values that correspond to certain percentages of stall torque, according to Equations (11) and (12). In addition, only PM losses were taken into account, as core losses are two orders of magnitude less than total PM losses, while having a greater computational cost. Figure 12 illustrates how, in this case study, the efficiency peaks at about 88% load. Total losses for the case of 88% of the stall torque are 5.5% lower than for the case of full load.
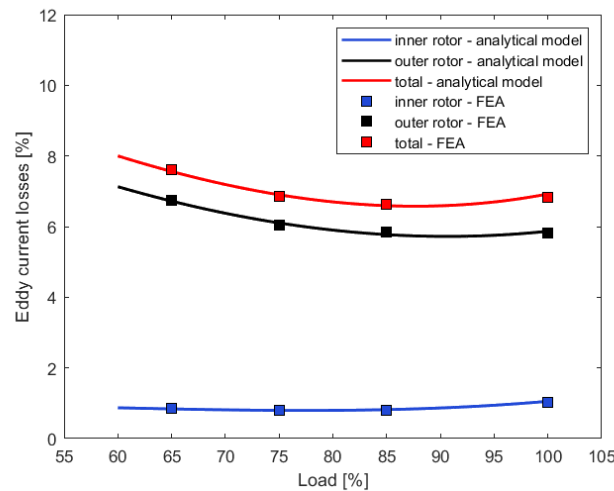
Figure 12. PM power losses as a percentage of total power transmitted vs. external load.

The analytical results were verified and found to be in excellent coherence with the FEA. Overall, deviances between the two methods do not exceed 1.5%.

3.3. Algorithm Computational Cost vs. Accuracy

For the calculation of the eddy current losses, a full period as defined from Θ_p^k is required. However, the developed model requires time steps throughout one complete period of the system. In addition, the hybrid model for the calculation of core losses requires a meshing technique that could significantly increase the computational cost. Therefore, it is important to investigate how the computational cost could be reduced without losing accuracy in the obtained results.

3.3.1. Reduction in Time Steps

To reduce computational time, it is investigated whether a period is needed to compute the power losses with adequate accuracy or if the losses converge sooner than that. Therefore, in Equations (15) and (16), the time of the integration t_s will be investigated. The value of t_s can range between 0 and T. It is noted that the time step used remains the same in all cases, and it is equal to the time it takes for the inner rotor to rotate by $2°$ and, equivalently, for the outer rotor to rotate by $0.8°$.

The average PMs and core losses are calculated for various t_s values. Figure 13 illustrates that the power losses converge rapidly. The computational time cost can be reduced by a factor of 5, with a deviation of less than 2% from the results obtained for a complete period.
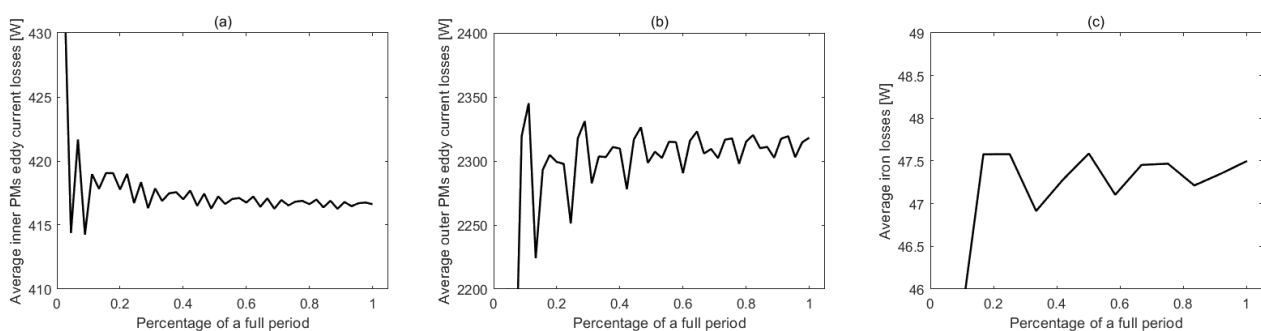

Figure 13. Average power losses versus the percentage of a complete period used to calculate them: (**a**) inner PMs, (**b**) outer PMs, (**c**) ferromagnetic segments.

3.3.2. Mesh Sensitivity Analysis

A mesh sensitivity analysis on the adopted mesh on the ferromagnetic segments is conducted in order to find the optimal mesh resolution that provides accurate core loss results in minimal computational time. Starting from a 10×10 grid and gradually reaching a 120×120 grid, it is found that for a very coarse mesh, the computed value of the core losses is significantly larger than their true value, and for finer meshes, the computed losses decrease and converge, as shown in Figure 14.
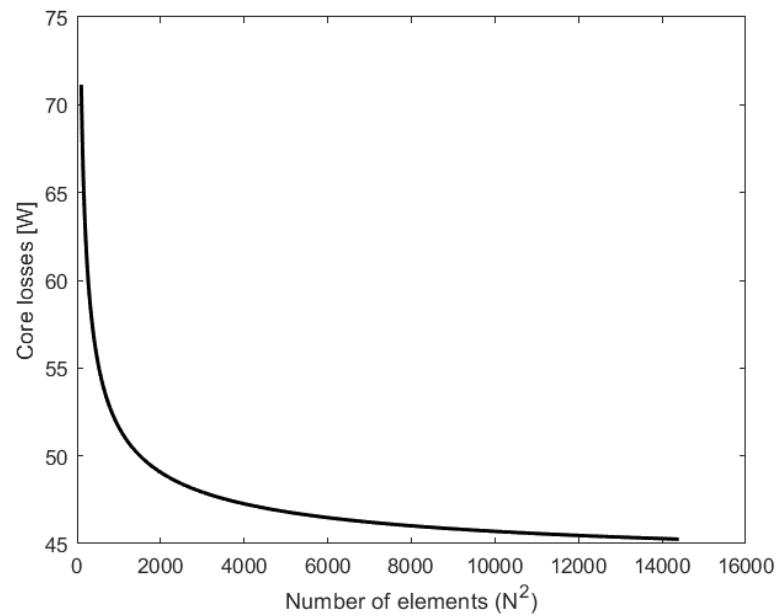
Figure 14. Convergence of core losses using mesh sensitivity analysis.

Grids ranging from 10×10 to 40×40 do not significantly increase the computational time, as solving the system of N^2 equations requires less time than calculating the flux density values on the boundary of the ferromagnetic segments, as obtained by [7]. However, the finer the meshes become, the more time consuming the computations become, as it is known that solving a system of linear equations can have a complexity of up to $O(N^3)$.

Coarse meshes lead to greater computed core losses because, as shown in Figure 10, the largest values of flux density and the corresponding time derivatives, which define the losses, are concentrated in small areas near the edges and corners of each ferromagnetic segment. This means that a coarse mesh attributes a large value of $\frac{dB_{maj}}{dt}$ and $\frac{dB_{min}}{dt}$ to a relatively large element, resulting in greater computed core losses. Thus, it is imperative that areas near the edges of the ferromagnetic segments have a mesh that is fine enough to accurately determine the flux density distribution. Future research could conduct a mesh sensitivity analysis with a focus on utilizing finer mesh near the boundaries and gradually transitioning to coarser mesh towards the center, where flux density is generally smoother, to reduce a significant percentage of computational time.

4. Conclusions

In the present work, an analytical 2D model is used to calculate eddy current losses in the PMs of a coaxial magnetic gear, as well as their minimization using magnet segmentation. A hybrid model is used to calculate the core losses in the ferromagnetic segments of the flux-modulator ring. The model utilizes the analytically computed values of the scalar magnetic potential on the boundaries of the segments and uses Laplace's equation in order to compute the magnetic flux density throughout the segments for the calculation of the core losses. Both models are validated using a transient FEA simulation, which shows a convergence of 1.51% and 3.18% for the eddy current and core losses, respectively, for an

indicative inner rotor speed of 2500 rpm. It was demonstrated that as expected, the total power losses increase as the rotational speed increases. The segmentation of the PMs was shown to play a crucial role in reducing the eddy current losses. The method showed that by performing just two segmentations on the outer rotor PMs, the overall losses decrease by over one order of magnitude. In addition, an investigation of the effect of the initial positioning of the rotors shows that peak efficiency is achieved at about 88% load in the performed case study. Finally, an attempt to reduce computational time while keeping the accuracy high is conducted by proving that only a small fraction of the period of the system is needed in order to accurately calculate total losses and by performing a mesh sensitivity analysis on the adopted grid of the ferromagnetic segments. The results of the average power losses throughout one full period illustrate the rapid convergence of power losses in a period, which can reduce the computational time by 80% with negligible errors. The mesh sensitivity analysis shows that mesh resolution is crucial for accurate core loss calculation, as meshes that are too coarse result in inaccurately high core losses and meshes that are too fine result in very high computational costs. These two analyses are of great importance, as they ensure high accuracy and relatively low computational costs simultaneously, facilitating optimization efforts. The developed model could be a valuable optimization tool for the reduction in power losses since it combines high accuracy and a low computational cost.

Author Contributions: Conceptualization, N.N. and P.T.; methodology, N.N., P.T., V.G. and C.P.; validation, N.N., P.T., V.G. and C.P.; investigation, N.N., P.T. and V.G.; writing—original draft, N.N., P.T., V.G., C.P., A.T. and V.S. All authors have read and agreed to the published version of the manuscript.

Data Availability Statement: Data are available on request from the authors.

Conflicts of Interest: The authors declare no conflicts of interest.

References

1. Tlali, P.M.; Wang, R.-J.; Gerber, S. Magnetic gear technologies: A review. In Proceedings of the 2014 International Conference on Electrical Machines (ICEM), Berlin, Germany, 2–5 September 2014; pp. 544–550.
2. Ruiz-Ponce, G.; Arjona, M.A.; Hernandez, C.; Escarela-Perez, R. A Review of Magnetic Gear Technologies Used in Mechanical Power Transmission. *Energies* **2023**, *16*, 1721. [CrossRef]
3. Atallah, K.; Howe, D. A novel high-performance magnetic gear. *IEEE Trans. Magn.* **2001**, *37*, 2844–2846. [CrossRef]
4. Belkhir, K.S.; Khenfer, N. Magnetic gear generator for wind energy. *Prz. Elektrotechniczny* **2013**, *89*, 72–75.
5. Johnson, M.; Gardner, M.C.; Toliyat, H.A.; Englebretson, S.; Ouyang, W.; Tschida, C. Design, construction, and analysis of a large-scale inner stator radial flux magnetically geared generator for wave energy conversion. *IEEE Trans. Ind. Appl.* **2018**, *54*, 3305–3314. [CrossRef]
6. Scheidler, J.J.; Asnani, V.M.; Tallerico, T.F. NASA's Magnetic Gearing Research for Electrified Aircraft Propulsion. In Proceedings of the AIAA/IEEE Electric Aircraft Technologies Symposium, Cincinnati, OH, USA, 12–14 July 2018.
7. Tzouganakis, P.; Gakos, V.; Kalligeros, C.; Tsolakis, A.; Spitas, V. Fast and efficient simulation of the dynamical response of coaxial magnetic gears through direct analytical torque modelling. *Simul. Model. Pr. Theory* **2023**, *123*, 102699. [CrossRef]
8. Desvaux, M.; Sire, S.; Hlioui, S.; Ben Ahmed, H.; Multon, B. Development of a Hybrid Analytical Model for a Fast Computation of Magnetic Losses and Optimization of Coaxial Magnetic Gears. *IEEE Trans. Energy Convers.* **2018**, *34*, 25–35. [CrossRef]
9. Wang, J.; Atallah, K.; Chin, R.; Arshad, W.M.; Lendenmann, H. Rotor eddy-current loss in permanent-magnet brushless ac machines. *IEEE Trans. Magn.* **2010**, *46*, 2701–2707. [CrossRef]
10. Filippini, M. Magnetic gears numerical modelling and optimization. Available online: https://www.research.unipd.it/handle/11577/3425766 (accessed on 16 May 2024).
11. Deng, F. An improved iron loss estimation for permanent magnet brushless machines. *IEEE Trans. Energy Convers.* **1999**, *14*, 1391–1395. [CrossRef]
12. Hein, H.; Yue, S.; Li, Y. Comparative Core Loss Calculation Methods for Magnetic Materials under Harmonics Effect. *IOP Conf. Series: Mater. Sci. Eng.* **2019**, *486*, 012019. [CrossRef]
13. Lee, J.-I.; Shin, K.-H.; Bang, T.-K.; Kim, K.-H.; Hong, K.-Y.; Choi, J.-Y. Core-Loss Analysis of Linear Magnetic Gears Using the Analytical Method. *Energies* **2021**, *14*, 2905. [CrossRef]

14. Li, Y.; Zhu, J.; Yang, Q.; Lin, Z.W.; Guo, Y.; Zhang, C. Study on Rotational Hysteresis and Core Loss Under Three-Dimensional Magnetization. *IEEE Trans. Magn.* **2011**, *47*, 3520–3523. [CrossRef]
15. Mateev, V.; Marinova, I. Loss estimation of magnetic gears. *Electr. Eng.* **2020**, *102*, 387–399. [CrossRef]